Expand the effective carriers in solid polymer electrolytes via anion-hosting cathode

Zongjie Sun
School of Chemistry, Xi'an Jiaotong University
Kai Xi
University of Cambridge https://orcid.org/0000-0003-0508-7910
Jing Chen
School of Chemistry, Xi'an Jiaotong University
Amor Abdelkader
University of Cambridge https://orcid.org/0000-0002-8103-2420
Mengyang Li
Xi'an Jiaotong University
Yue Lin
Cavendish Laboratory, University of Cambridge
Qiu Jiang
University of Electronic Science and Technology of China
Yaqiong Su
Xi'an Jiaotong University
Ramachandran Kumar
University of Cambridge https://orcid.org/0000-0001-9223-2332
Shujiang Ding (dingsj@mail.xjtu.edu.cn)
School of Chemistry, Xi'an Jiaotong University

Article

Keywords: solid polymer electrolytes, energy storage, batteries

Posted Date: June 17th, 2021

DOI: https://doi.org/10.21203/rs.3.rs-583179/v1

Version of Record: A version of this preprint was published at Nature Communications on June 9th, 2022. See the published version at https://doi.org/10.1038/s41467-022-30788-5.

Abstract

The non-reactive anion migration deteriorates the limited ionic conductivity of the solid polymer electrolytes (SPEs) and accelerates solid-state batteries failure. Here, we introduce an integrated approach in which polyvinyl ferrocene (PVF) cathode encourage anions and Li^+ to act as effective carriers simultaneously. The concentration polarization and poor rate performance, caused by insufficient effective carriers, were addressed by the participation of anions in electrode reaction. Specifically, the PVF|Li battery matched with unmodified SPE (PEO-LiTFSI) showed 107 mAh g^{-1} initial capacity at 100 μA cm^{-2} and maintained 70% retention for more than 2800 cycles at 300 μA cm^{-2} and 60°C. Moreover, the slight capacity decrease at 1000 μA cm^{-2} and the successful batteries operation at minimal ionic conductivity (8.13×10^{-6} S cm^{-1}) show that the current carrying capacity of SPEs was greatly improved without complex design. This strategy weakens the strict requirements for ion conductance and interface engineering of SPEs, and provides an efficient scenario for constructing advanced polymer-based all-solid-state batteries.

Main

The safety requirement for lithium-ion batteries and the demand for lithium metal anode has prompted researchers to look for solid-state alternatives to liquid organic electrolytes[1-3]. Since Wright and coworkers reported the ionic conductivity of the mixture of polyethylene oxide (PEO) and alkali metal salts[4], solid polymer electrolytes (SPEs) had been considered as a potential solution for constructing all-solid-state lithium secondary batteries[5,6]. However, the weak polymer chain motion leads to insufficient ion transport for SPEs even at high temperature[3,6]. Many investigators have committed to developing high ion conductive SPEs. Typical strategies include designing the polymer segment structure[7,8] and combining polymer matrix with ceramic [9,10] or inorganic solid electrolytes[11-13].

One critical problem that has to be solved for constructing advanced SPEs is the movement of anions. The dissociation of lithium salt in SPEs depends on the dipolar interaction between the polymer chain (e.g., $-CH_2-CH_2-O-$ in PEO) and Li^+[14,15]. Similar to the liquid electrolyte, the large solvation structure significantly slows the migration of Li^+[16,17]. In contrast, the non-coordinating anions contribute most of the ionic conductance in SPEs, meaning that the majority of ion migration is irrelevant to energy generation. Hence, the rate performance of polymer-based solid-state batteries was restricted to a great extent by the limited effective carrier concentration. Another issue caused by anion migration is concentration polarization, attributed to anions aggregation on the electrode surface during cycles[18,19]. This polarization results in critical performance degradation, such as increasing internal resistance and decreasing operating voltage[20], most importantly, promoting lithium metal dendrite growth[21]. The short-circuit in polymer-based solid-state batteries generally predates the combination of liquid components and commercial separators, which runs counter to the original intention of solid-state electrolytes. Single-ion conducting solid polymer electrolytes (SISPEs) was suggested to alleviate the problems caused by

anion migration[22,23]. By constructing polymer segments with weak interaction with Li^+[24] or grafting anions to the polymer backbone[25], SISPEs can achieve high t_{Li+} (>0.9). However, this comes at the cost of ionizing less free Li^+ and also the low ionic conductivity due to the lack of solvation ability.

The participation of anions in electrode reaction has promoted the development of attractive energy conversion systems in the liquid or extended gel phase[26-28]. These systems were intended as low-cost alternatives to lithium-ion batteries, focus on some key parameters such as sustainability and material availability[29,30]. Apart from the requirement for high electrochemical stability, the electrolyte of the anion reaction system is similar to that of lithium-ion batteries. The benefit of the effective carrier expansion is hidden by the abundant ionic conductivity of the liquid/gel electrolyte. However, for solvent-free SPEs with limited ion movement, the strategy of enhancing the correlation between ion migration and electrode reaction is expected to play a more crucial role. In this work, we introduced anion-hosting cathode to overcome the negative impact owing to non-reactive anion migration in SPEs. The ferrocene unit, anchored to the long-chain polymer, encourage anions as the effective charge carrier similar to Li^+. The expansion of carriers significantly improves current carrying capacity of unmodified SPEs (Fig. 1), and avoids the short-circuit failure lead by concentration polarization. Besides, the impact of anion species on ion mobility and interacting with the cathode is also investigated in depth.

Materials design and characterization

The electronic structure of the cyclopentadiene and iron atom hybrid orbital provides ferrocene with stable and reversible redox properties (Fig. 2b)[31,32]. To avoid the diffusion of active units in a non-flow system, we anchored the anion-hosting unit to the polymer chain by free-radical polymerization of vinyl ferrocene, as illustrated in Fig. 2a. The EDX mapping proves the homogeneous distribution of Fe element across the PVF. The polymerization process was confirmed by the Fourier transform infrared spectroscopy (FT-IR) in Fig. 2c, which shows a significant weakening of double bond vibration peaks at 1625 cm^{-1} after polymerization. The gel permeation chromatography (GPC) results (Table S1) prove that PVF has a high molecular weight (~4800 g mol^{-1}) with wide distribution (M_w/M_n = 1.71). The redox of PVF can provide a theoretical capacity of 124 mAh g^{-1} (Fig. 2d), locating at the top level of the anion-hosting organic cathode[33,34]. Moreover, the theoretical redox potential of ~3.45 V vs. Li^+/Li can be tolerated by most SPEs. The thermogravimetric analysis (TGA) in Fig. S1 shows that PVF did not undergo significant thermal weight loss or phase change below 300 °C, ensuring the electrode stability in the case of high temperature operation.

Classic SPEs are composed of lithium salt and polymer with solvation ability. Benefiting from the high dielectric constant and chain flexibility, PEO is one of the most widely studied polymers matrix[10,11,35]. Based on the well-designed anion hosting material, the PVF|Li battery matched with PEO-LiTFSI electrolyte exhibits excellent cycle stability. It maintained 70 % capacity retention after 2800 cycles (Figure 2e) at 60 °C, while avoiding battery failure for more than 4000 cycles (Figure 2e, 2f). Considering the current case, where the migration of anions and cations is related to the electrodes' reaction, we set

several types of lithium salt in SPEs to obtain a deep insight into the anion electrode reaction. The ionic conductivity of the SPEs was conducted through AC impedance (seen in Fig. S2). Fig. S3 plots the ionic conductivity as a function of temperature. Owing to the high delocalized negative charge of anions, PEO-LiTFSI displays the highest ionic conductivity (3.53×10^{-4} S cm^{-1} at 333 K). Except for $LiClO_4$, other electrolytes have comparable conductivity at high temperature. The differential scanning calorimetry (DSC) results of SPEs correspond to the ionic conductivity, where PEO-LiTFSI has the lowest melting point (Fig. S4).

Inefficient utilization of ions in SPEs severely restrict the batteries performance. To explore the ion mobility influence in the designed systems, we measured the lithium-ion transference number (t_{Li+}) of SPEs through the steady-state current method (results are shown in Fig. S5, Table S2). As seen in Fig. 3a, the electrolytes with LiTFSI, LiFSI and $LiClO_4$ as salts pose low t_{Li+} which are all-around 0.1, proving that anions contribute the most ion movement in these SPEs. Note that the calculated t_{Li+} of PEO-LiBOB electrolyte is negative (-0.38) differ from other threes. In fact, negative cation transfer numbers are not rare, and usually attributed to the presence of ionic aggregates[36,37]. As shown in Fig. 3b, while the negatively charged ion clusters dominate the charge transfer in electrolyte, the t_{Li+} of SPEs can be low to negative due to the short-range interactions[38,39]. The domination of ion clusters could reduce the carrier loading capacity at high current density, which affects the battery performance, as will be discussed later. The AC impendence results of PVF|Li batteries shown in Fig. 3c proves that negatively charged clusters significantly increase the batteries' charge transfer resistance with PEO-LiBOB electrolytes, despite the high ionic conductivity compared to other SPEs. Generally, for a typical Li^+-hosting cathode, SPE with low t_{Li+} operate poorly. However, the anions participation in the electrode reaction breaks through the strict requirement on ion aggregation in the SPEs[20]. The PVF|Li batteries assembled with SPEs all exhibit reversible charge-discharge process shown in Fig. 3d, and the overpotential of batteries is controlled by the ion conductivity of SPEs. Moreover, the anion species lead a difference on operating voltage of batteries. This finding prompted us to further study of anion impact.

Anion impact on electrode reaction

The electrochemical stability of the SPEs was evaluated using Li|SPE|stainless steel cells. The linear scanning voltammetry (LSV) curves in Fig. S6 shows a low redox current within a voltage window up to 4 V vs. Li^+/Li, ensuring that the electrode reaction is not disturbed by electrolyte oxidation. The electrochemical behavior of PVF with anions was evaluated through cyclic voltammetry (CV) tests. As shown in Fig. 4a, the PVF cathode shows good redox reversibility provided by the active unit. Notably, the stabilization of the unit into polymer engages a crucial role in the electrode reaction reversibility. With the free ferrocene electrode (Fig. S7), even with a high content of the conductive agent, the assembled solid-state battery exhibits oxidation peak only in the first cycle. This indicates that the ion pair formed by ferrocenium and anion cannot undergo further reduction. In contrast, PVF with its long-chain structure prevents the diffusion of active materials by anchored ion pairs into the polymer. The peak potential separation (ΔE) shown in CV results is informative of the electrochemical reaction kinetics. Judging from

Fig. 4c, the highest ionic conductivity SPE, PEO-LiTFSI, has the lowest potential gap (ΔE = 0.103 V), while PEO-$LiClO_4$ has the highest ΔE (Fig. 3d), corresponding to the ionic conductance trend.

The influence of anion species on the electrode reaction in liquid electrolyte, related to anion couples, was previously investigated by Redepenning et al[40]. The results show that the ion pairs' formation could negative shift the electrode potential from theoretical[41,42]. To determine the ion pair effect on the electrode in SPEs, we conducted density functional theory (DFT) simulations to calculate the binding energy (BE) of different anions to the cathode. The cathode was simplified by substituting ethyl ferrocenium for the polyvinyl ferrocenium (Table S4). The calculations indicated that ethyl ferrocenium has the highest BE to ClO_4^-, and decrease with the order FSI^-, BOB^-, and $TFSI^-$ (Fig. 4b). However, the experimental results are telling a different story. Apart from the PEO-$LiClO_4$, the batteries with PEO-LiTFSI and PEO-LiBOB electrolytes exhibit high electrode potential close to theoretical with small difference, which are 3.464 and 3.466 V, respectively. And, the FSI^- lead the electrode potential to drop slightly to 3.443 V. Considering the steric hindrance of the polymer chain can further explain the contradiction. Unlike the small ethyl ferrocenium monomer considered in the DFT calculation, the folded long-chain polyvinyl ferrocenium suppress the combination of large anions, weakening the effect of ion-pairing on the electrode potential. Therefore, ClO_4^-, with the smallest structure (shown in Fig. S8) and the strongest BE among four anions (Fig. 4b), significantly shift the electrode potential to negative (3.383 V vs. Li^+/Li) while the larger anions are not significantly affected by the binding effect. Before further examining the all-solid-state batteries, we evaluated the capacity and stability of the PVF electrode with liquid electrolyte (1.0 M $LiPF_6$ in EC/DMC wt %). The capacity increase in the first five cycles can be attributed to the cathode electrochemical activation, previously observed in several organic electrodes[43]. The initial capacity of 113 mAh g^{-1} and high retention of capacity in 100 cycles (Fig. S9) exhibit the stable redox property of PVF. Besides, the combination of PF_6^- and cathode also shifts voltage plateau to a lower value (~3.27 V) than the theoretical, which can be explained by the combined effects discussed above.

Enhanced batteries rate performance and anode stability

Motivated by the results that the batteries with PEO-LiTFSI and PEO-LiBOB electrolytes have small polarization and high capacity (Fig. 3d), we focused on these two SPEs for further studies of long cycles. After a few cycles of cathode activation in PEO-LiBOB electrolyte, the PVF capacities were measured to be 112, 104, and 107 mAh g^{-1} at currents of 20, 50, and 100 μA cm^{-2}, respectively (Fig. S10). The capacity has not been significantly attenuated after a long period cycling. However, as shown in Fig. S11, the battery with PEO-LiBOB electrolyte shows substantial polarization and significant capacity fade at higher current density (~67 mAh g^{-1} at 300 μA cm^{-2}), which is as weak as the SPEs containing ClO_4^- and FSI^- (Fig. S12), despite the ionic conductance disparity among threes. The poor rate performance of batteries with LiBOB salt can be ascribed to the formation of ions aggregations demonstrated in the previous section. The sluggish electrode reaction deteriorates the battery performance at high current densities.

Benefit from high ionic conductivity, large anion structure and the ability to prevention aggregation, the battery with PEO-LiTFSI showed excellent cycle stability and rate performance (Fig. S13, S14). Specifically, the initial capacity reaches 97 mAh g^{-1} at 300 μA cm^{-2} and maintained 90 % after 1000 cycles (Fig. 2e). Benefiting from the extended carriers, the battery exhibits good rate performance, with capacities of 108, 107, 97, and 94 mAh g^{-1} at current densities of 100, 200, 300, and 500 μA cm^{-2}, respectively (Fig. 5f). Even when the current increases to 1 mA cm^{-2}, which is intolerable by many reported advanced SPEs, the battery still maintains 78 mAh g^{-1} capacity with a stable plateau. The PVF electrode exhibits pseudo-capacitance, which also contributes to the excellent rate performance to a certain extent (Fig. S15). It is worth noting that the electrode reaction rate is not the rate-determining step of most solid-state device owing to the limited ion transport capability of solid electrolytes. Despite using a large amount of the conductive agent to overcome PVF low conductivity, the result of the control experiment proves that the capacity contribution of the conductive agent at the tested voltage range is negligible (Fig. S16). The decrease of conductive agent proportion reduces the battery's rate performance significantly (Fig. S17). However, this does not affect the effectiveness of the strategy proposed in this report. The extended carrier makes the ionic conductivity of SPEs no longer a bottleneck of the battery’s performance at high current loading. The addition of single-walled carbon nanotubes in the electrode can significantly increase the proportion of active materials with the reduced polarization (Fig. S18), which provides massive space for the high conductive anion-hosting electrode.

Concentration polarization could induce serious consequences in SPEs when only Li^+ act as effective carriers, significantly accelerate anode degradation and battery failure especially at high current density (Fig. 5b). Taking the charging process as an example, the Li^+-hosting cathode (e.g., $LiFePO_4$) undergoes an anodic reaction. In an ideal situation, the ion number in SPEs keep constant throughout the process. The concentration of Li^+ increase on the cathode side and decrease on the counter. This leads to a salt concentration gradient and ion diffusion barriers (Fig. S19a). The SPEs can be regarded as liquid electrolyte with extremely high viscosity. The minimal ion diffusion results in a stable massive concentration gradient, which is more severe than that in liquid. In the present work where anions were involved in energy storage, the ions and ions clusters migration under electric field is similar to that of $LiFePO_4$. The difference between two cases is that the PVF electrode reaction consumes anions similar to Li^+ on the anode in SPEs (Fig. 5a). Therefore, the distribution of SPEs salt concentration is homogeneous, facilitating the ions' diffusion and avoiding the detrimental consequences of the concentration polarization (Fig. S19b).

To verify that minimizing the concentration polarization could effectively enhance the lithium anode stability, we tested $LiFePO_4$|PEO-LiTFSI|Li batteries under the same condition (Fig. S20). As shown in Fig. 5c, 5e, a micro short circuit occurred in $LiFePO_4$|Li at the 24th hour at 300 μA cm^{-2}. The short circuit has not been repaired in subsequent cycles, leading to a continuous decayed in coulombic efficiency (Fig. S20b). Similar failures are common in other polymer-based solid-state batteries, even for SPEs with improved ionic conductivity and interface properties. In contrast, the coulombic efficiency of the PVF|PEO-

LiTFSI|Li battery maintained about 99.7 % with no short circuit observed over 4000 cycles at 300 μA cm^{-2} (Fig. 5c, d), which is the maximum level for most polymer-based solid-state-batteries. The excellent cycle stability proves the success of our concept in controlling the polarization and suppressing lithium anode deterioration.

Performance with insufficient ionic conductivity

As an unmodified SPE, the combination of PEO-LiTFSI does not have advantages in terms of ionic conductivity and interfacial properties, usually performed as negative comparison. However, the expansion of the effective carrier through the anion-hosting cathode eliminates the demand of complex design for advanced SPEs. We compared the rate performance of this work with the reported advanced SPEs in Fig. 5g[35,44-51]. The strategy we proposed strongly enhances capacity retention at high current density with simple PEO-LiTFSI without any modifications, better than other SPEs of complex design (details in Table S5).

The improvement of the current-carrying capacity of SPEs inspired us to examine the battery performance with very low ionic conductance. PEO-LiTFSI exhibits extremely limited ionic conductivity of 2.65×10^{-7} S cm^{-1} at 30 °C, far from the usual battery test requirement. In this condition, PVF|Li batteries exhibited capacities of 83, 60, 48 mAh g^{-1} at 10, 30, and 50 μA cm^{-2} with increased polarization, respectively (Fig 6c). The inferior ionic conductivity leads the unsatisfactory performance. As an ideal additive, succinonitrile (SN) could strengthen the segment movement ability of polymer thereby enhancing SPEs' ionic conductivity[52,53]. After doping PEO-LiTFSI with 5% SN, the ionic conductivity increased to 8.13×10^{-6} S cm^{-1} at 30 °C (Fig. S21a). Therefore, the battery assembled by PEO-LiTFSI-SN electrolyte show a lower impedance compared with the electrolyte without plasticizer (Fig. S21b). The CV curves exhibit stable and reversible redox performance (Fig. 6a). As shown in Fig. 6b, 6c, the recorded capacities at 10, 30, and 50 μA cm^{-2} rise to 94, 86, and 70 mAh g^{-1}, respectively. The PVF|Li batteries with these two SPEs both maintain more than 100 cycles at 30 μA cm^{-2} without significant capacity decayed. The anion-hosting cathode makes full use of each dissociated ion in electrolytes, resulting in a battery system with high tolerance to SPEs with very low ionic conductivity. In short, this strategy avoids plenty problems devoted to the low ionic conductivity and utilization faced by previous reported SPEs[5,6,23] (Fig. 6d), reinforcing the correlation between ion movement and electrode reaction.

Discussion

In summary, we developed advanced polymer-based solid-state batteries by inducing anions as effective carriers simultaneously with Li^+. The anion-hosting cathode PVF put the entire ion movement of SPEs into energy storage, which produces an updated rate performance and promotes batteries operation at very limited ionic conductance. In addition, the ultra-stable cycles of PVF|Li batteries prove that the anode deterioration, mainly contributed by concentration gradients, were avoided effectively by reactive anion migration, which is essential in building safer metal anode batteries. Besides, experiments and theoretical

calculations clarified the effects of anion structure, binding energy and ion aggregation on battery performance. This work provides a pioneering strategy for the design of advanced solid-state energy storage systems. However, future investigations into high capacity and conductivity anion-hosting cathode are certainly warranted. Since the migration and aggregation of anions differ from Li^+ in most SPEs, the disparity of reaction status between cathode and anode could present some minor complications and addressing this issue could be the subject of the following study.

Materials And Methods

Materials

PEO (Mw=6×10^5), LiTFSI (99%), LiFSI (99%), $LiClO_4$ (99.9%), LiBOB (98%) were purchased from Aladdin. Vinyl ferrocene (98%) was purchased from Meryer. 2,2'-azoisobutyronitrile (AIBN) was recrystallized before use. PVDF (HSV900), conductive agent (Super P) and separator (Celgard 2325) were fully dried before use. $LiFePO_4$ and liquid electrolyte were purchased from DoDoChem. N-methyl pyrrolidone (NMP) and acetonitrile were of analytical grade and used directly without further purification. Dry toluene was obtained from a VSPS-5 solvent purification system.

Synthesis of polyvinyl ferrocene and solid polymer electrolytes

Polyvinyl ferrocene (PVF) was synthesized by free-radical polymerization. In a typical process, vinyl ferrocene was dissolved in dry toluene, and AIBN was used as the initiator. The ratio of [monomer] / [Initiator] = 100, $[monomer]_0$ = 2 M. The reaction was continued at 60 °C for 48 hours. The obtained dark red solution was washed with a large amount of methanol and dried under vacuum to obtain yellow powder.

Polyethylene oxide and lithium salts were dissolved in acetonitrile. The obtained solution was coated on a polytetrafluoroethylene plate and dried under reduced pressure to obtain a self-supported film. The electrolyte membrane was kept in Ar atmosphere glove box to prevent moisture contamination. The solid electrolyte containing succinonitrile adopts the same preparation method.

Materials characterization

The thermal gravimetric analysis was carried out with METTLER TOLEDO TGA/DSC^{3+} at a temperature range of 30-800 °C under nitrogen atmosphere, with a heating rate of 10 K min^{-1}. Fourier transform infrared (FT-IR, Bruker Tensor 27) were recorded between 400 and 4000 cm^{-1}. A field emission scanning electron microscope (FE-SEM, SU-6600) equipped with an energy dispersive spectrometer was used to characterize the samples' morphology. All the electrochemical characterization was performed using the electrochemical workstation (PARSTAT 1000 and CHI 660E).

Electrochemical measurements

The active material (PVF), conductive agent (Super P) and binder (PVDF) were dispersed in N-methyl pyrrolidone at a ratio of 4: 5: 1 or 6: 3: 1. The dispersed slurry was coated on aluminum foil and dried under reduced pressure at 60 °C. The prepared electrodes were stored in a glovebox until use. The same method was used to prepare $LiFePO_4$ electrodes with a ratio of 7:2:1 and the Super P electrode in a ratio of 85:15 (conductive agent: binder). The mass loading of the active material was controlled at 1.0 mg cm^{-2}. The electrodes were cut into discs (d = 12 mm) for subsequent testing. The cells assembly was carried out in a glove box filled with argon gas (H_2O, O_2 < 0.1 ppm), using metallic lithium as the counter electrode.

The ionic conductivity of the electrolyte was measured by sandwiching the polymer electrolyte film between two stainless steel electrodes and then record the electrochemical impedance. The ionic conductivity was calculated by the following equation

$$\sigma = \frac{l}{RS}$$

l is the thickness of the polymer electrolyte, **R** is the bulk resistance of the polymer electrode, and **S** is the electrolyte area.

The electrochemical impedance spectroscopy (EIS) of the batteries was tested under an open circuit with a frequency range of 10^{-1}-10^5 Hz. The cyclic voltammetry (CV) and linear sweep voltammetry (LSV) test were performed at a scan rate of 0.2 mV s^{-1}. Galvanostatic charge/discharge tests were performed within a voltage window of 2.8~4 V (v.s. Li/Li^+) on a LAND battery tester.

DFT computational methods

All of the optimization and frequency calculations were carried out on the B3LYP/6-311+G(d,p) level, and the optimized structures are free from imaginary frequency. The binding energies were calculated by $E_{binding} = E_{compound} - E_{anion} - E_{cation}$. The results are shown in Table S4. All of the above calculations were carried out with Gaussian 16 program package.

Declarations

Acknowledgments

Funding: This research was supported in part by the National Natural Science Foundation of China (Nos. 51773165, and 51973171), and Young Talent Support Plan of Xi'an Jiaotong University. Natural Science Basic Research Program of Shaanxi (No. 2020-JC-09). China Postdoctoral Science Foundation (2019M663687), Fundamental Research Funds for the Central Universities (xjh012020042).

Competing interests: The authors declare that they have no competing interests.

Data and materials availability: All data needed to evaluate the conclusions in the paper are present in the paper and/or the Supplementary Materials. Additional data related to this paper may be requested from the authors.

References

1. M. Armand, J. M. Tarascon, Building better batteries. *Nature* **451**, 652-657 (2008).

2. J. B. Goodenough, K. S. J. A. C. S. Park, The Li-ion rechargeable battery: A perspective *J. Am. Chem. Soc.* **135**, 1167-1176 (2013).

3. A. Manthiram, X. W. Yu, S. F. Wang, Lithium battery chemistries enabled by solid-state electrolytes. *Nat. Rev. Mater.* **2**, 16103 (2017).

4. D. E. Fenton, J. M. Parker, P. V. Wright, Complexes of alkali-metal ions with poly(ethylene oxide). *Polymer* **14**, 589-589 (1973).

5. J. Mindemark, M. J. Lacey, T. Bowden, D. Brandell, Beyond PEO-alternative host materials for Li^+-conducting solid polymer electrolytes. *Prog. Polym. Sci.* **81**, 114-143 (2018).

6. D. Zhou, D. Shanmukaraj, A. Tkacheva, M. Armand, G. X. Wang, Polymer electrolytes for lithium-based batteries: advances and prospects. *Chem-Us* **5**, 2326-2352 (2019).

7. R. Khurana, J. L. Schaefer, L. A. Archer, G. W. Coates, Suppression of lithium dendrite growth using cross-linked polyethylene/poly(ethylene oxide) electrolytes: A new approach for practical lithium-metal polymer batteries. *J. Am. Chem. Soc.* **136**, 7395-7402 (2014).

8. J. Lopez, Y. Sun, D. G. Mackanic, M. Lee, A. M. Foudeh, M. S. Song, Y. Cui, Z. Bao, A dual-crosslinking design for resilient lithium-ion conductors. *Adv. Mater.* **30**, 1804142 (2018).

9. W. Liu, N. Liu, J. Sun, P. C. Hsu, Y. Li, H. W. Lee, Y. Cui, Ionic conductivity enhancement of polymer electrolytes with ceramic nanowire fillers. *Nano Lett.* **15**, 2740-2745 (2016).

10. W. Liu, S. W. Lee, D. Lin, F. Shi, S. Wang, A. D. Sendek, Y. Cui, Enhancing ionic conductivity in composite polymer electrolytes with well-aligned ceramic nanowires. *Nat. Energy* **2**, 17035 (2017).

11. H. Zhai, P. Xu, M. Ning, Q. Cheng, J. Mandal, Y. Yang, A flexible solid composite electrolyte with vertically aligned and connected ion-conducting nanoparticles for lithium batteries. *Nano Lett.* **17**, 3182-3187 (2017).

12. Z. Xue, T. Liu, S. Zhang, H. Xin, B. Xu, Y. Lin, B. Xu, L. Li, C. W. Nan, S. Yang, Synergistic coupling between $Li_{6.75}La_3Zr_{1.75}Ta_{0.25}O_{12}$ and poly(vinylidene fluoride) induces high ionic conductivity, mechanical strength and thermal stability of solid composite electrolytes. *J. Am. Chem. Soc.* **139**, 13779 (2017).

13. Jin, Zheng, Dr., Mingxue, Tang, Prof., Yan-Yan, Hu, Lithium ion pathway within $Li_7La_3Zr_2O_{12}$-polyethylene oxide composite electrolytes. *Angew. Chem. Int. Ed.* **55**, 12538-12542 (2016).

14. M. A. Ratner, D. F. Shriver, Ion-transport in solvent-free polymers. *Chem. Rev.* **88**, 109-124 (1988).

15. M. Li, C. Wang, Z. Chen, K. Xu, New concepts in electrolytes. *Chem. Rev.* **120**, 6783-6819 (2020).

16. O. Borodin, G. D. Smith, Mechanism of ion transport in amorphous poly(ethylene oxide)/LiTFSI from molecular dynamics simulations. *Macromolecules* **39**, 1620-1629 (2006).

17. D. Diddens, A. Heuer, O. Borodin, Understanding the Lithium Transport within a Rouse-Based Model for a PEO/LiTFSI Polymer Electrolyte. *Macromolecules* **43**, 2028-2036 (2010).

18. I. Rey, J. Lassègues, P. Baudry, H. Majastre, Study of a lithium battery by confocal Raman microspectrometry. *Electrochimica Acta* **43**, 1539-1544 (1998).

19. I. Rey, J. L. Bruneel, J. Grondin, L. Servant, J. C. Lassegues, Raman spectroelectrochemistry of a lithium/polymer electrolyte symmetric cell. *J. Electrochem. Soc.* **145**, 3034-3042 (1998).

20. M. Doyle, T. F. Fuller, J. Newman, The Importance of the Lithium Ion Transference Number in Lithium Polymer Cells. *Electrochimica Acta* **39**, 2073-2081 (1994).

21. M. Rosso, C. Brissot, A. Teyssot, M. Dolle, L. Sannier, J. M. Tarascon, R. Bouchetc, S. Lascaud, Dendrite short-circuit and fuse effect on Li/polymer/Li cells. *Electrochimica Acta* **51**, 5334-5340 (2006).

22. R. Bouchet, S. Maria, R. Meziane, A. Aboulaich, L. Lienafa, J. P. Bonnet, T. N. T. Phan, D. Bertin, D. Gigmes, D. Devaux, R. Denoyel, M. Armand, Single-ion BAB triblock copolymers as highly efficient electrolytes for lithium-metal batteries. *Nat. Mater.* **12**, 452-457 (2013).

23. H. Zhang, C. Li, M. Piszcz, E. Coya, T. Rojo, L. M. Rodriguez-Martinez, M. Armand, Z. Zhou, Single lithium-ion conducting solid polymer electrolytes: advances and perspectives. *Chem. Soc. Rev.* **46**, 797-815 (2017).

24. K. M. Diederichsen, E. J. Mcshane, B. D. Mccloskey, The most promising routes to a high Li^+ transference number electrolyte for lithium ion batteries. *ACS Energy Lett.* **2**, 2563-2575 (2017).

25. D. Zhou, A. Tkacheva, X. Tang, B. Sun, D. Shanmukaraj, P. Li, F. Zhang, M. Armand, G. Wang, Stable conversion chemistry-based lithium metal batteries enabled by hierarchical multifunctional polymer electrolytes with near-single ion conduction. *Angew. Chem. Int. Ed.* **58**, 6001 –6006 (2019).

26. C. Yang, J. Chen, X. Ji, T. P. Pollard, X. Lu, C. J. Sun, S. Hou, Q. Liu, C. Liu, T. Qing, Aqueous Li-ion battery enabled by halogen conversion–intercalation chemistry in graphite. *Nature* **569**, 245-250 (2019).

27. M. C. Lin, M. Gong, B. Lu, Y. Wu, D. Y. Wang, M. Guan, M. Angell, C. Chen, J. Yang, B. J. Hwang, H. Dai, An ultrafast rechargeable aluminium-ion battery. *Nature* **520**, 325-328 (2015).

28. X. F. Xu, K. Lin, D. Zhou, Q. Liu, X. Y. Qin, S. W. Wang, S. He, F. Y. Kang, B. H. Li, G. X. Wang, Quasi-solid-state dual-ion sodium metal batteries for low-cost energy storage. *Chem.* **6**, 902-918 (2020).

29. W. Meng, C. Jiang, S. Zhang, X. Song, Y. Tang, H. M. Cheng, Reversible calcium alloying enables a practical room-temperature rechargeable calcium-ion battery with a high discharge voltage. *Nat. Chem.* **10**, 667–672 (2018).

30. G. Chen, F. Zhang, Z. Zhou, J. Li, Y. Tang, A flexible dual-ion battery based on PVDF-HFP-modified gel polymer electrolyte with excellent cycling performance and superior rate capability. *Adv. Energy Mater.* **8**, 1801219 (2018).

31. Y. Zhao, Y. Ding, J. Song, G. Li, G. B. Dong, J. B. Goodenough, G. H. Yu, Sustainable electrical energy storage through the ferrocene/ferrocenium redox reaction in aprotic electrolyte. *Angew. Chem. Int. Ed.* **53**, 11036-11040 (2014).

32. H. Bo, C. Debruler, Z. Rhodes, T. L. Liu, Long-cycling aqueous organic redox flow battery (AORFB) toward sustainable and safe energy storage. *J. Am. Chem. Soc.* **139**, 1207-1214 (2016).

33. Z. P. Song, H. S. Zhou, Towards sustainable and versatile energy storage devices: an overview of organic electrode materials. *Energy Environ. Sci.* **6**, 2280-2301 (2013).

34. Y. Lu, J. Chen, Prospects of organic electrode materials for practical lithium batteries. *Nat. Rev. Chem.* **4**, 127-142 (2020).

35. J. Wan, J. Xie, X. Kong, Z. Liu, K. Liu, F. Shi, A. Pei, H. Chen, W. Chen, J. Chen, X. Zhang, L. Zong, J. Wang, L. Q. Chen, J. Qin, Y. Cui, Ultrathin, flexible, solid polymer composite electrolyte enabled with aligned nanoporous host for lithium batteries. *Nat. Nanotechnol.* **14**, 705-711 (2019).

36. T. Xie, A. France-Lanord, Y. Wang, Y. Shao-Horn, J. C. Grossman, Graph dynamical networks for unsupervised learning of atomic scale dynamics in materials. *Nat. Commun.* **10**, 2667 (2019).

37. H. K. Kim, N. P. Balsara, V. Srinivasan, Continuum description of the role of negative transference numbers on ion motion in polymer electrolytes. *J. Electrochem. Soc.* **167**, 110559 (110511pp) (2020).

38. D. M. Pesko, K. Timachova, R. Bhattacharya, M. C. Smith, I. Villaluenga, J. Newman, N. P. Balsara, Negative transference numbers in poly(ethylene oxide)-based electrolytes. *J. Electrochem. Soc.* **164**, E3569-E3575 (2017).

39. A. France-Lanord, J. C. Grossman, Correlations from ion-pairing and the Nernst-Einstein equation. *Phys. Rev. Lett.* **122**, 136001 (2018).

40. J. Redepenning, E. Castro-Narro, G. Venkataraman, E. Mechalke, Influence of supporting electrolyte activity on formal potentials measured for dissolved internal standards in acetonitrile. *J. Electrochem. Soc.* **498**, 192-200 (2001).

41. K. Uosaki, Y. Sato, H. Kita, Electrochemical characteristics of a gold electrode modified with a self-assembled monolayer of ferrocenylalkanethiols. *Langmuir* **7**, 1510-1514 (1991).

42. G. Inzelt, L. Szabo, The effect of the nature and the concentration of counter ions on the electrochemistry of poly(vinylferrocene) polymer film electrodes. *Electrochimica Acta* **31**, 1381-1387 (1986).

43. Y. Wang, Y. Deng, Q. Qu, X. Zheng, J. Zhang, G. Liu, V. S. Battaglia, H. Zheng, Ultrahigh-capacity organic anode with high-rate capability and long cycle life for lithium-ion batteries. *ACS Energy Lett.* **2**, 2140-2148 (2017).

44. W. Zhou, Z. Wang, Y. Pu, Y. Li, J. B. Goodenough, Double-layer polymer electrolyte for high-voltage all-solid-state rechargeable batteries. *Adv. Mater.* **31**, 1805574 (2019).

45. H. Wang, Q. Wang, X. Cao, Y. He, K. Wu, J. Yang, H. Zhou, W. Liu, X. Sun, Thiol-branched solid polymer electrolyte featuring high strength, toughness, and lithium ionic conductivity for lithium-metal batteries. *Adv. Mater.* **32**, 2001259 (2020).

46. D. G. Mackanic, W. Michaels, M. Lee, D. W. Feng, J. Lopez, J. Qin, Y. Cui, Z. N. Bao, Crosslinked poly(tetrahydrofuran) as a loosely coordinating polymer electrolyte. *Adv. Energy Mater.* **8**, 1800703 (2018).

47. Y. Liu, R. Hu, D. Zhang, J. Liu, M. Zhu, Constructing Li-rich artificial SEI layer in alloy-polymer composite electrolyte to achieve high ionic conductivity for all solid-state lithium metal batteries. *Adv. Mater.* **33**, 2004711 (2021).

48. C. K. Zhang, Z. H. Niu, J. Bae, L. Y. Zhang, Y. Zhao, G. H. Yu, Polyeutectic-based stable and effective electrolytes for high-performance energy storage systems. *Energy Environ. Sci.* **14**, 931-939 (2021).

49. Q. Liu, D. Zhou, D. Shanmukaraj, P. Li, F. Y. Kang, B. H. Li, M. Armand, G. X. Wang, Self-Healing Janus interfaces for high-performance LAGP-based lithiummetal batteries. *ACS Energy Lett.* **5**, 1456-1464 (2020).

50. P. Jaumaux, Q. Liu, D. Zhou, X. Xu, T. Wang, Y. Wang, F. Kang, B. Li, G. Wang, Deep-Eutectic-solvent-based self-healing polymer electrolyte for safe and long-life lithium-metal batteries. *Angew. Chem. Int. Ed.* **132**, 9219 – 9227 (2020).

51. M. Martinez-Ibaez, E. Sanchez-Diez, L. Qiao, Y. Zhang, H. J. A. F. M. Zhang, Unprecedented improvement of single Li-ion conductive solid polymer electrolyte through salt additive. *Adv. Funct. Mater.*

30, 2000455 (2020).

52. P. J. Alarco, Y. Abu-Lebdeh, A. Abouimrane, M. Armand, The plastic-crystalline phase of succinonitrile as a universal matrix for solid-state ionic conductors. *Nat. Mater.* **3**, 476-481 (2004).

53. L. Z. Fan, Y. S. Hu, A. J. Bhattacharyya, J. Maier, Succinonitrile as a Versatile Additive for Polymer Electrolytes. *Adv. Funct. Mater.* **17**, 2800-2807 (2010).

Figures

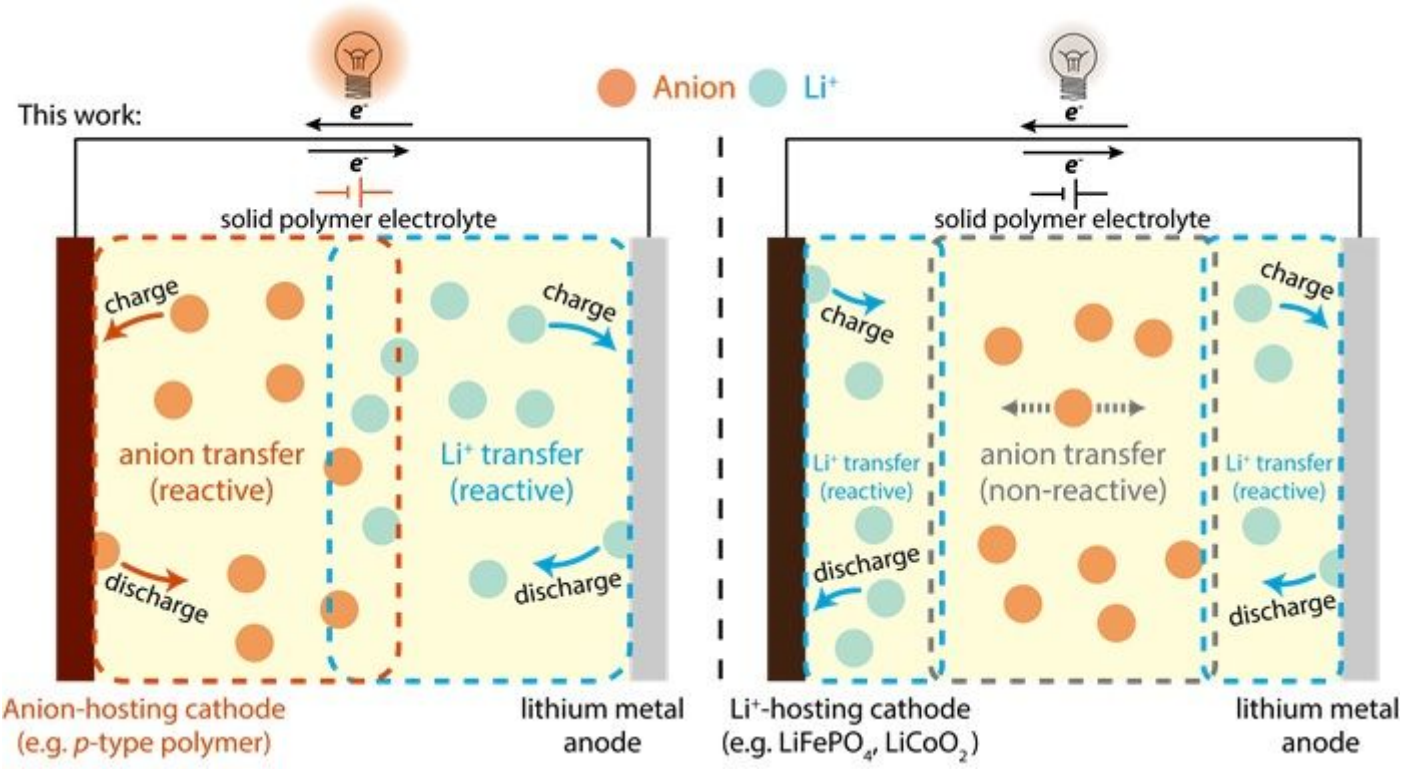

Figure 1

Anion and cation migration and electrode reaction. The ions transfer in SPEs of all-solid-state batteries using different ion acceptors as the cathode (left: anion-hosting cathode (this work), e.g., p-type polymer, right: Li+-hosting cathode).

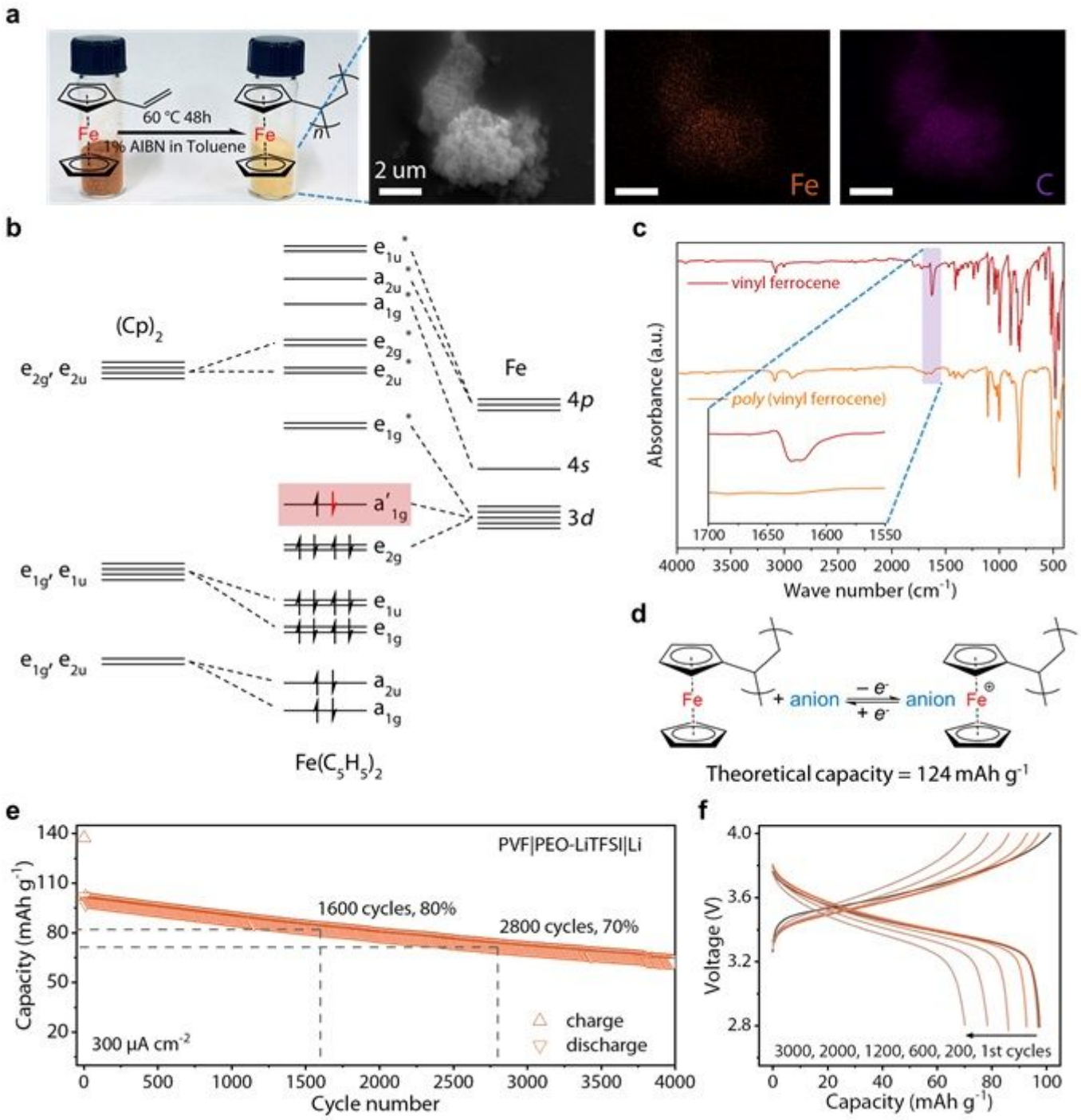

Figure 2

Synthesis and redox properties of polyvinyl ferrocene. (a) The optical image, SEM image and elemental mapping results of the polyvinyl ferrocene, and the color change significantly after polymerization. (b) The frontier orbital electronic structure of ferrocene/ferrocenium, while the electron transfer in the redox reaction is marked in red. (c) FT-IR Spectroscopy of vinyl ferrocene and polyvinyl ferrocene and the inset shows the weakening of the peak intensity at 1625 cm-1. (d) The electrode redox reaction of PVF with electrolyte anions, where the theoretical capacity is based on the molecular weight of the active unit and

the charge transfers numbers. (e), (f) show the capacity retention and charge-discharge curves of PVF|Li battery at 60 °C, 300 μA cm-2, respectively. The battery was cycled at 50 μA cm-2 in the first 5 cycles.

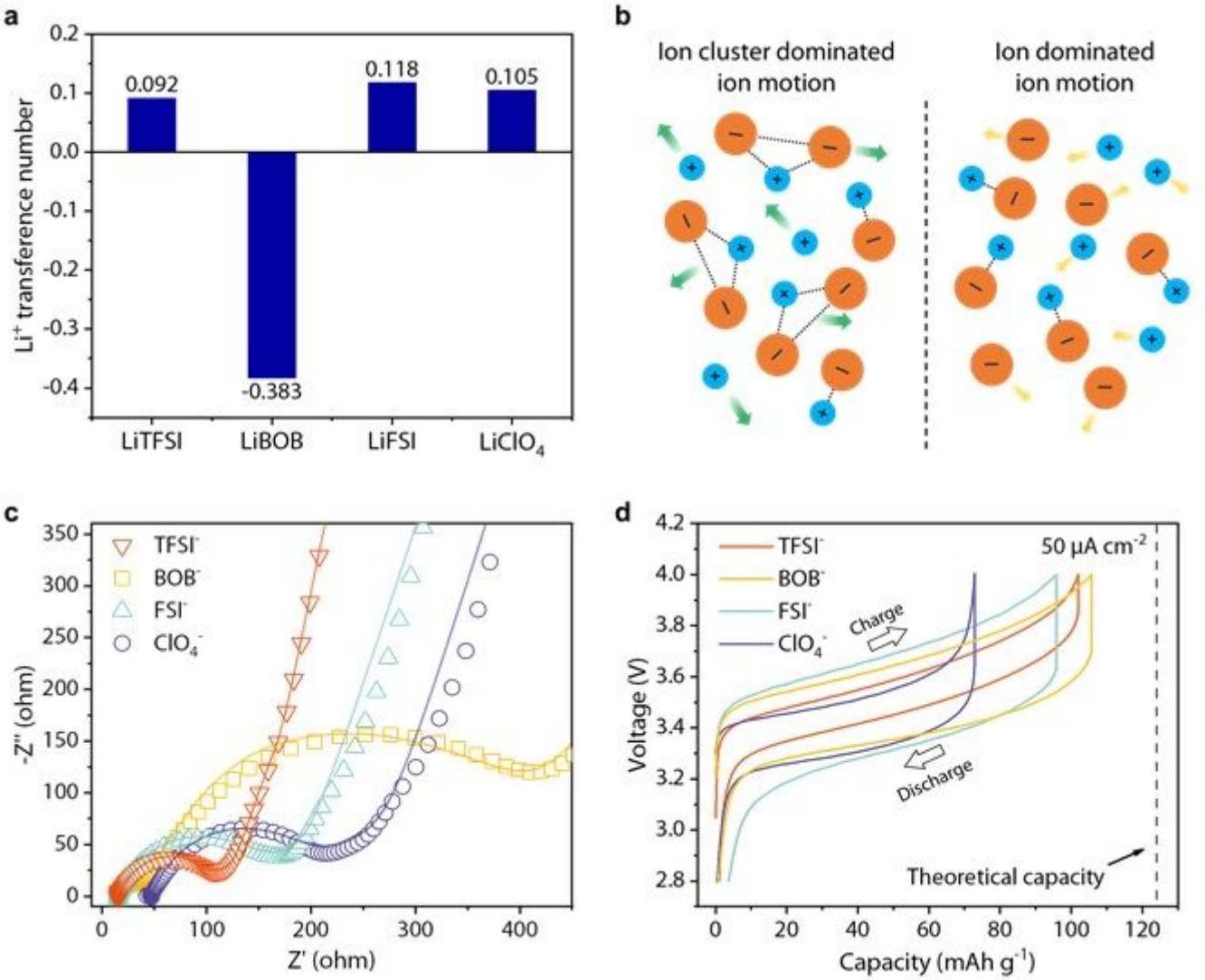

Figure 3

Ion aggregation in SPEs and the impact on battery performance. (a) Lithium-ion transference number performed by steady-state current method (b) Ion motion in SPEs dominated by aggregated ion cluster (left) and single ion (right), where dashed lines between ions represent short-range intracluster interactions and arrows correspond to the ion motion considered in SPEs. Considering ion cluster as noninteracting species provide an approximation more precise than the usual Nernst-Einstein equation to the tLi+, able to explain the mechanism responsible for the negative value36,39. (c) Nyquist plots of PVF|Li batteries with different anion species before cycles, and the solid line represent the impendence fitting results. (d) Charge-discharge curves of PVF|Li batteries performed at 50 μA cm-2, the theoretical capacity was marked as a dashed line.

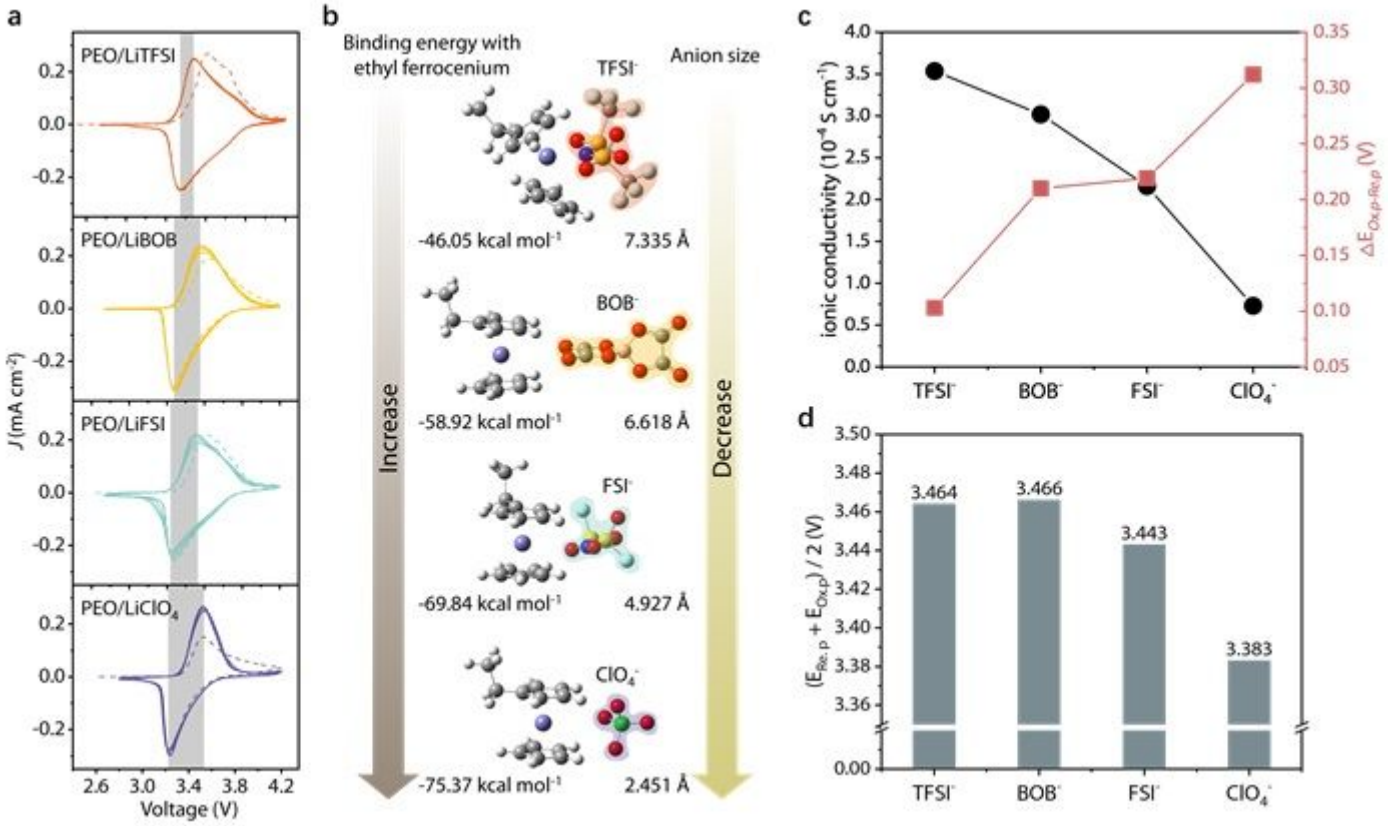

Figure 4

Electrode reaction affected by anion species. (a) Cyclic voltammetry curves of PVF|Li batteries constructed with different SPEs in five cycles, and the dashed line indicate the first cycle. The gray parts show the disparity of ΔE in the electrode reaction. (b) The anions' binding energy with ethyl ferrocenium and size trends. (c) The negative correlation between the ionic conductivity of electrolyte and ΔE at 60 °C. (d) The electrode potential of PVF|Li batteries, calculated by the average of oxidation and reduction peak in CV results.

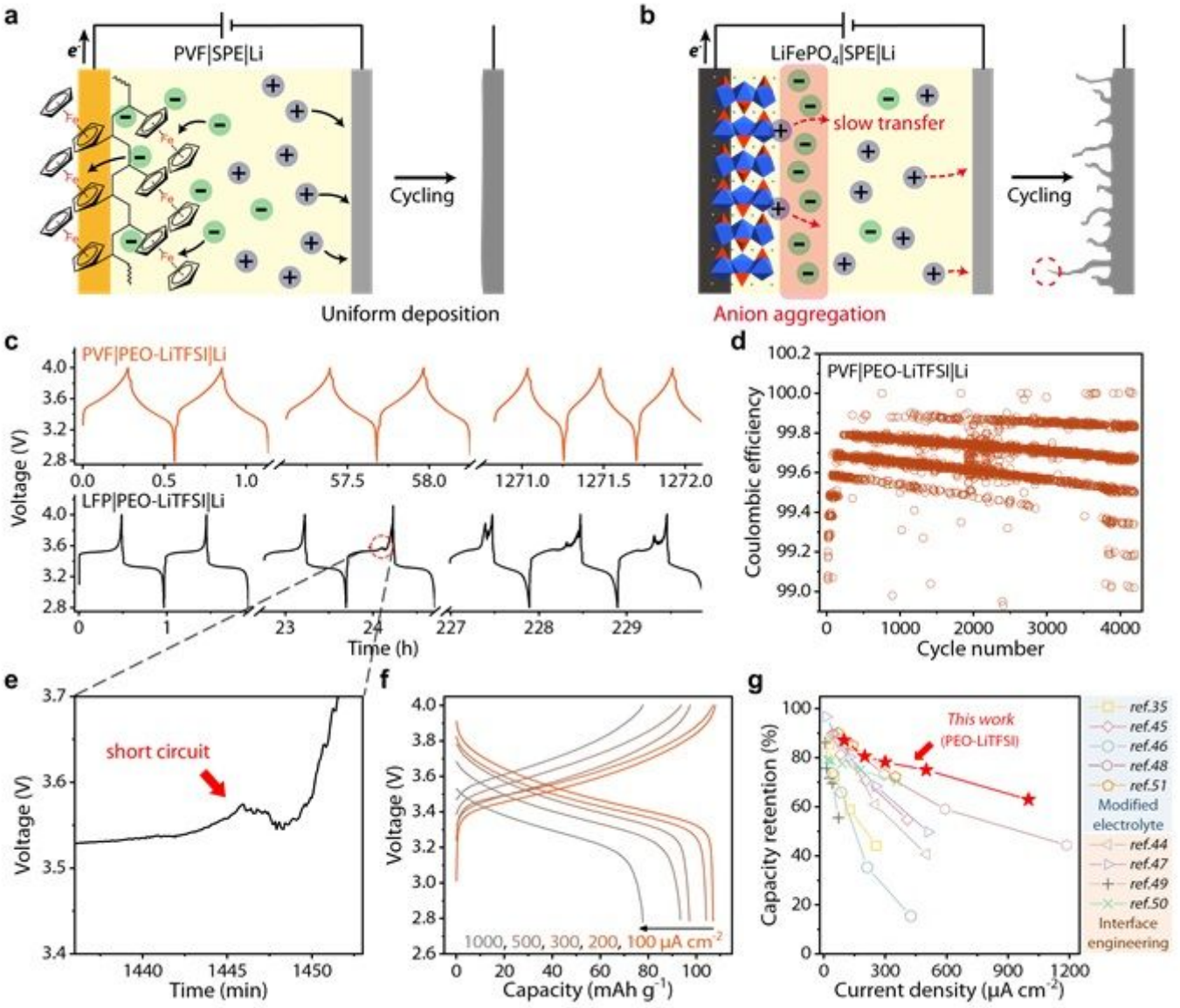

Figure 5

Carrier expansion improves rate performance and cycle stability. Schematic diagram of anode morphology changes during cycling where (a) PVF and (b) LiFePO4 served as the cathode. (c) The voltage change curves of PVF|Li (top) and LFP|Li (bottom) batteries with time at 300 μA cm-2 and (d) Coulombic efficiency of PVF|Li battery over 4000 cycles (e) Magnified view of voltage change with time during LFP|Li battery cycles (f) The rate performance from 100 to 1000 μA cm-2 and (g) the comparison between this work and the other reported advanced SPEs, classified in the graph by design strategy (detail seen in Table S5).

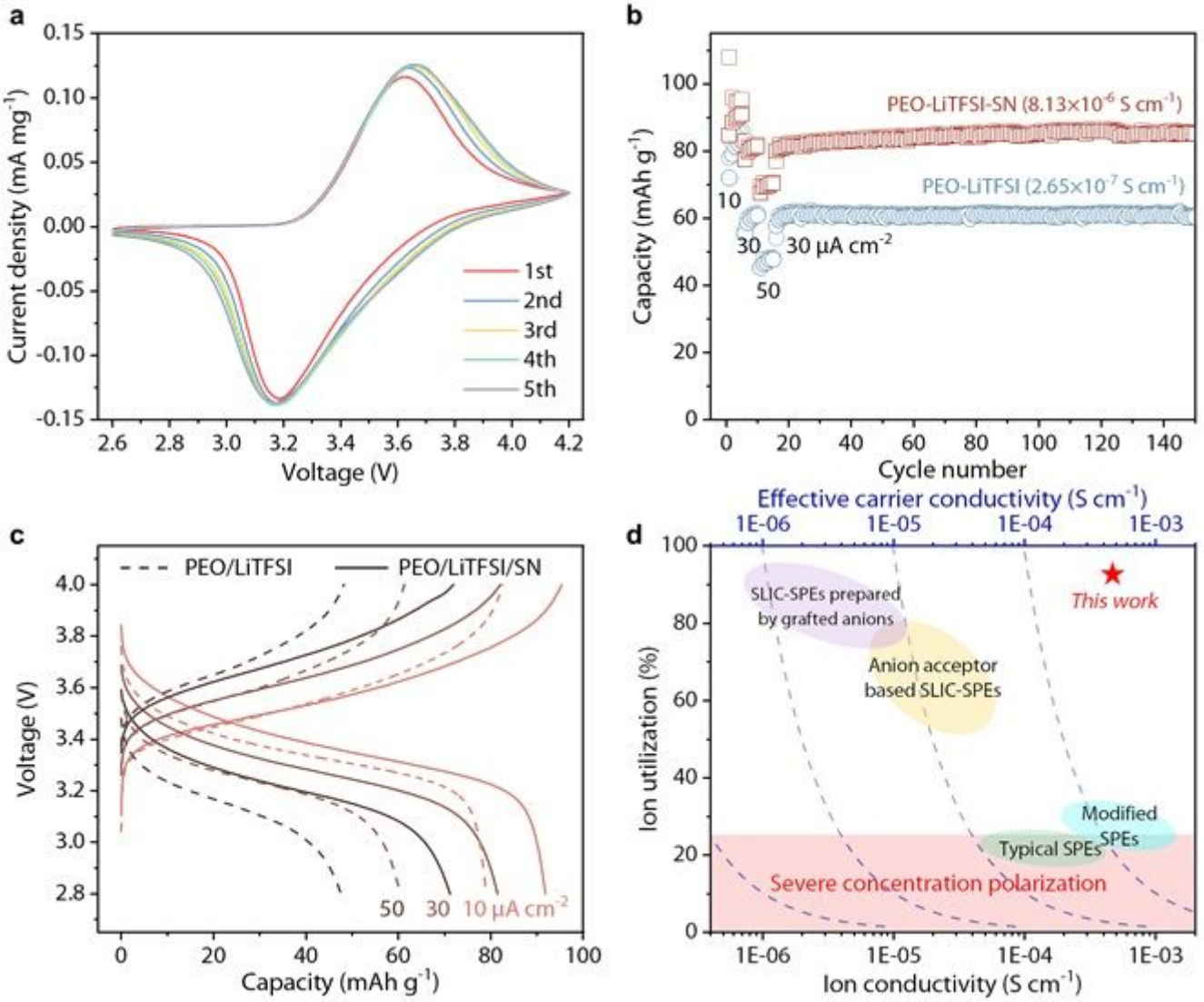

Figure 6

PVF|Li Batteries performance with insufficient ionic conductance SPEs (a) Cyclic voltammetry curves of PVF|Li battery at 0.2 mV s-1 assembled with 5 wt% SN added SPE at 30 °C (b) The cycle performance and (c) charge-discharge curves of PVF|Li battery with 10, 30, 50 μA cm-2, respectively (d) Comparison of the effective carrier number of this work and other types of polymer-based solid electrolytes, where the ionic conductivity was specifically collected at batteries operating temperature.

Supplementary Files

This is a list of supplementary files associated with this preprint. Click to download.

- SupplementaryMaterials.docx